Electronic Supplementary Material (ESI) for Energy & Environmental Science

Electronic Supplementary Information

for

Edge-carboxylated graphene nanoplatelets as oxygen-rich metal-free cathodes for organic dye-sensitized solar cells

Myung Jong Ju,[a,‡] In-Yup Jeon,[d,‡] Kimin Lim,[b,‡] Jae Cheon Kim,[c] Hyun-Jung Choi,[d] In Taek Choi,[a] Yu Kyung Eom,[a] Young Jin Kwon,[a] Jaejung Ko,[b,*] Jae-Joon Lee,[c,*] Jong-Beom Baek[d,*] and Hwan Kyu Kim[a,*]

[a]*Global GET-Future Lab. & Department of Advanced Materials Chemistry, Korea University, Sejong 339-700, Korea. E-mail: hkk777@korea.ac.kr.*

[b]*Photovoltaic Materials, & Department of Advanced Materials Chemistry, Korea University, Sejong 339-700, Korea. E-mail: jko@korea.ac.kr.*

[c]*Nanotechnology Research Center & Department of Applied Chemistry, Konkuk University, Chungju 380-701, Korea. E-mail: jjlee@knu.ac.kr.*

[d]*Interdisciplinary School of Green Energy/Low-Dimensional Carbon Materials Center, Ulsan National Institute of Science and Technology (UNIST), Ulsan 689-798, Korea. E-mail: jbbaek@unist.ac.kr.*

[‡]These authors contributed equally to this work.

Experimental details

Edge-carboxylated graphene nanoplatelets (ECGnPs). Graphite (5.0 g) and dry ice (100.0 g) were into a stainless steel capsule containing stainless steel balls (500.0 g) of 5 mm in diameter. The container was then sealed and fixed in the planetary ball-mill machine (Pulverisette 6), and agitated with 500 rpm for 48 h. There after, the built-up internal pressure was very slowly released through a gas outlet. Upon opening the container lid in air at the end of ball-milling, sparkling occurred due to the violent hydration reaction of carboxylates into carboxylic acids by the air moisture. The resultant product was further Soxhlet extracted with aqueous HCl (1 M) solution to completely acidify carboxylates and to remove metallic impurities, if any. Final product was freeze-dried at –120 °C under a reduced pressure (0.05 mmHg) for 48 h to yield ECGnPs (6.2 g) uptaken at least CO_2 (1.2 g) as dark black powder.

Reduced graphene oxide (rGO). Graphene oxide (GO) was prepared by using modified Hummers' process. In brief, graphite (3.0 g) was mixed with of $NaNO_3$ (1.5 g) and concentrated H_2SO_4 (75 mL). The mixture was cooled down to 0 °C in an ice bath and stirred for 2 h. Then, $KMNO_4$ (9.0 g) was added slowly, maintaining the temperature lower than 5 °C throughout the mixing. The mixture was continuously stirred for another hour and warmed up to room temperature by removing cooling bath. To the mixture, distilled water (100 mL) was added and the temperature was increased to 90 °C in an oil bath. Additional water (300 mL) was added and continuously stirred for another hour and a half. The color of the mixture turned to mud brown. This mixture was then treated with H_2O_2 (30%, 30 mL) and hot water (3 L) was added and diluted. The mixture was further washed with excess water until the pH of the filtrate was nearly neutral to yield graphene oxide (GO). The brown colored GO dispersion in water was reduced by using hydrazine monohydrate at 80 °C for 12 h. Black precipitation of reduced GO (rGO) was formed and collected by filteration using a

PTFE membrane (0.45 μm) and washed with plenty of water. The product was further purified by Soxhlet extraction with methanol, THF and water. Finally, the resultant rGO was freeze-dried under reduced pressure (0.5 mmHg) at −120 °C for 48 h.

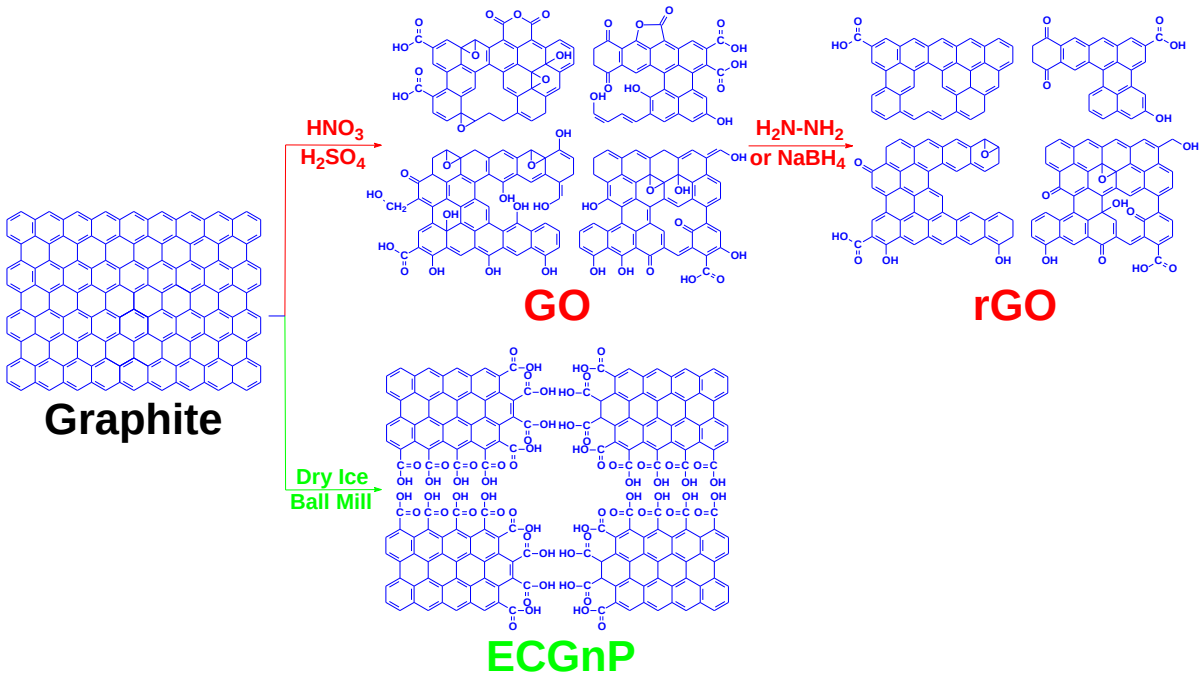

Fig. S1 Proposed structures of graphene oxide (GO), reduced graphene oxide (rGO) and edge-carboxylated graphene nanoplatelets (ECGnPs).

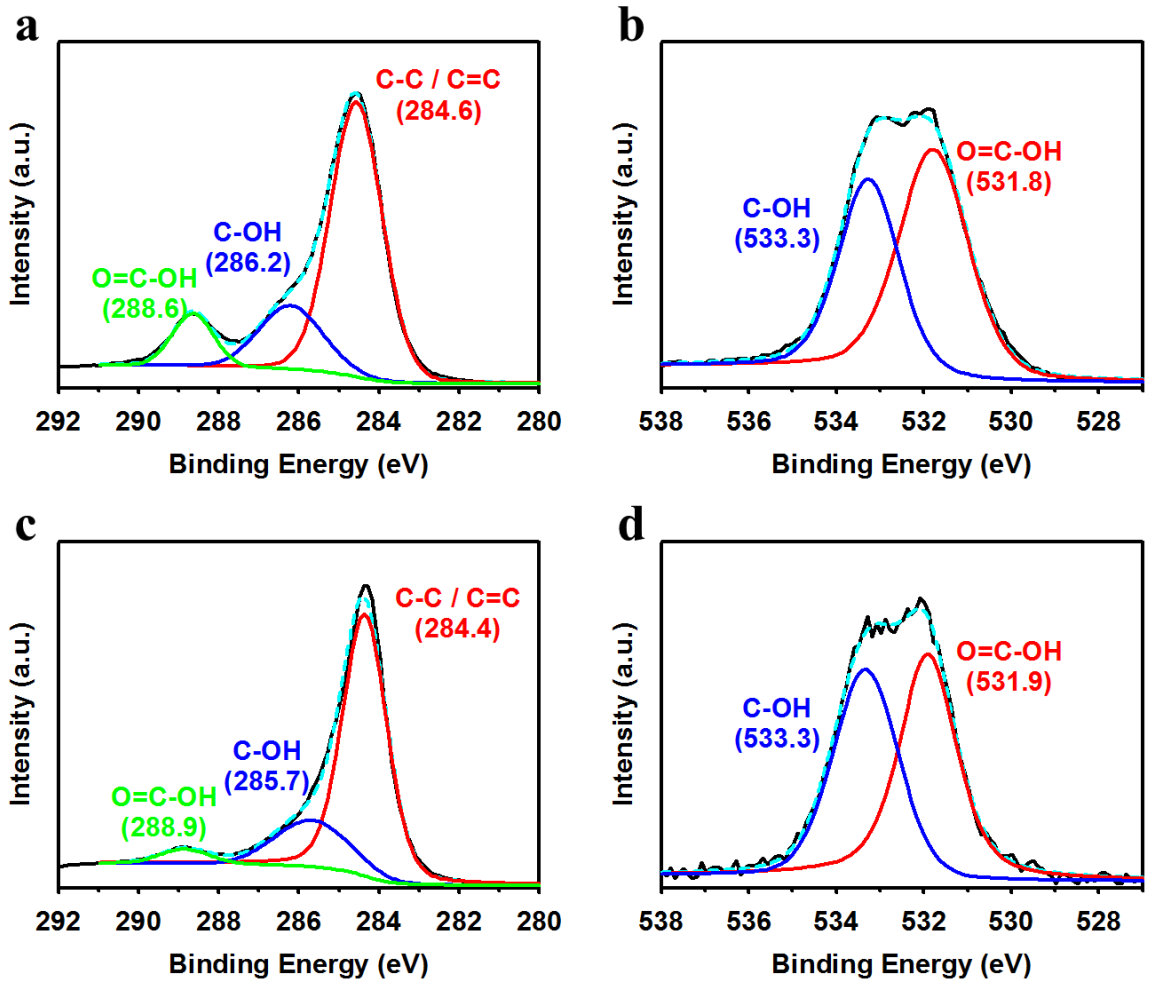

Fig. S2 High resolution XPS spectra: (a) C 1s (b) O 1s of ECGnP; (c) C 1s (d) O 1s of rGO.

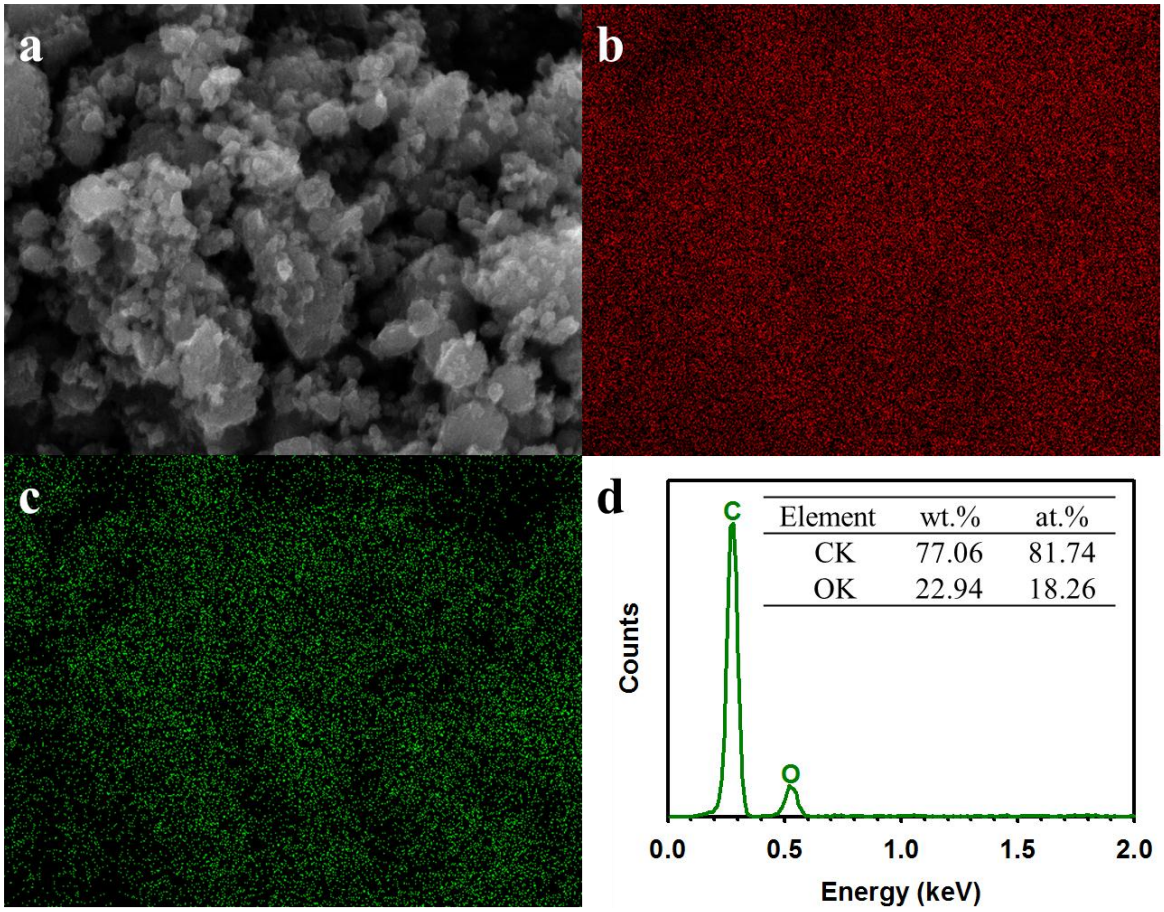

Fig. S3 SEM image and its corresponding EDX element mappings of ECGnP: (a) SEM image; (b) carbon mapping; (c) oxygen mapping; (d) EDX spectrum.

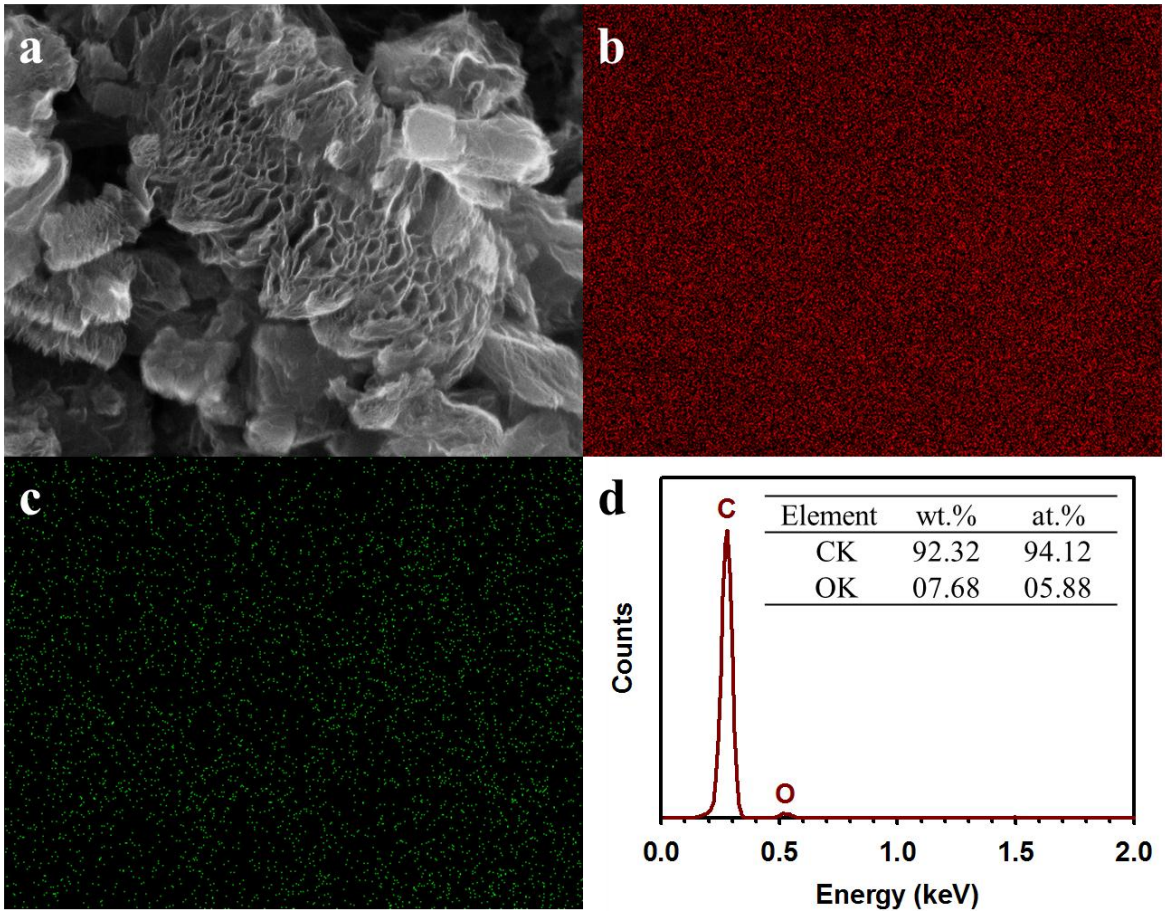

Fig. S4 SEM image and its corresponding EDX element mappings of rGO: (a) SEM image; (b) carbon mapping; (c) oxygen mapping; (d) EDX spectrum.

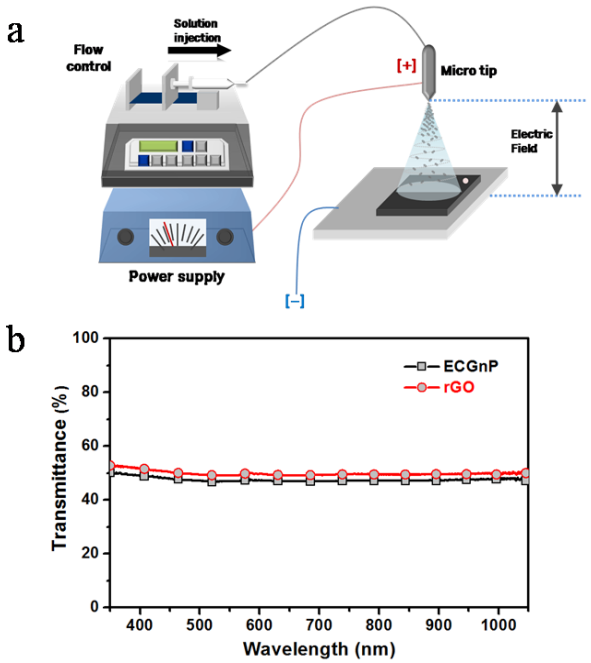

Fig. S5 (a) A schematic presentation of the e-spray setup for ECGnP and rGO deposition on the surface of FTO. (b) Optical transmittance of rGO and ECGnP films on FTO: about 49 and 50% for the ECGnP and rGO, respectively.

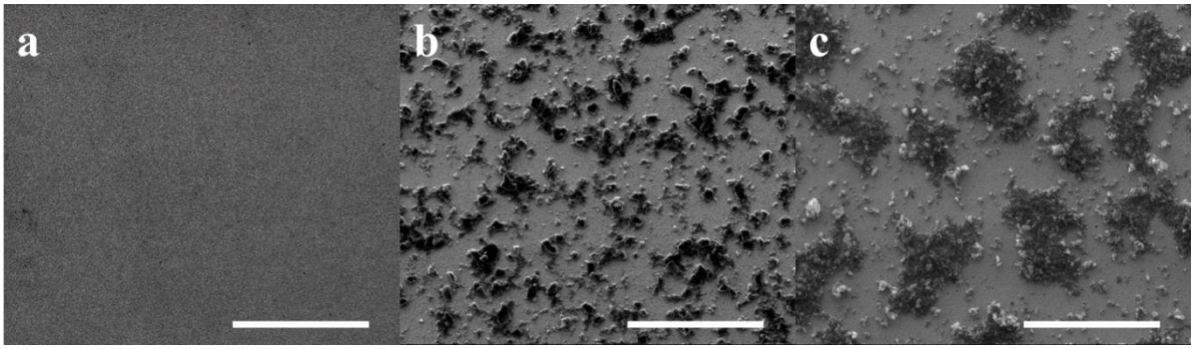

Fig. S6 SEM images: (a) the surface of bare FTO; (b) the surface of ECGnP deposited on FTO; (c) the surface of rGO deposited on FTO. Scale bars are 100 μm.

An equivalent circuit (EC) shown in **Fig. 3c**, which is well known as a Randles-type EC, where R_S is the ohmic serial resistance, R_{CT} is the charge transfer resistance at the CE/electrolyte solution interface, Z_W is the Nernst diffusion impedance in the bulk electrolyte

solution between the two identical electrodes, and CPE is a constant phase element due to the roughness of the electrode surface, the impedance spectrum of the CE/electrolyte interface deviates slightly from the behavior of a RC EC with an ideal capacitance.[S1] This effect can be described by a CPE, and the impedance Z_{CPE} of a CPE is:

$$Z_{CPE} = B(j\omega)^{-\beta} \qquad \text{(S1)}$$

where ω is the angular frequency, B (CPE parameter) and β (CPE exponent) are frequency independent parameters of CPE ($0 \leq \beta \leq 1$; for $\beta = 1$, the Z_{CPE} transforms into capacitance at the electrical double-layer). The Nernst impedance describes the diffusion of $Co(bpy)_3^{3+}$ in the electrolyte due to the large excess of $Co(bpy)_3^{2+}$ to $Co(bpy)_3^{3+}$. The diffusion coefficients of $Co(bpy)_3^{3+}$ and $Co(bpy)_3^{2+}$ are of the same order of magnitude, since $Co(bpy)_3^{2+}$ does not contribute to the diffusion impedance. The Nernst impedance Z_W to mass transfer (e.g., diffusion coefficient, D) is given by the Warburg impedance in the electrolyte solution as described in eq. (S2):

$$Z_W = \frac{W}{\sqrt{j\omega}} tanh\sqrt{\frac{j\omega}{K_N}} \qquad \text{(S2)}$$

where W is the Warburg parameter and K_N is $D/0.25\delta^2$.[S2] Fitting of the second semicircles at Nyquist plots shown in **Fig. 3b** to Z_W allow determination of the diffusion coefficient (D) of $Co(bpy)_3^{3+}$.

Owing to the pioneering work on the poly(3,4-ethylenedioxythiophene) (PEDOT) material for DSSCs,[S3] we have also adopted the conductive polymer of PEDOT:PSS (poly (3,4-ethylenedioxythiophene) : poly (styrenesulfonate)) as another reference CE in DSSCs. PEDOT-PSS (0.5 wt% PEDOT, 0.8 wt% PSS, Aldrich) was obtained from Aldrich and the solution was filtrated through 0.2 μm of filter membrane before use. To investigate of its electrocatalytic performance for $Co(bpy)_3^{2+/3+}$ redox couple, PEDOT:PSS/EtOH solution (v/v,

1/3) was deposited on FTO by using an e-spray technique. A voltage of ~ 9 kV was applied between a metal orifice and the conducting substrate at a distance of 3.5 cm. The feed rate was controlled at a constant flow rate of 50 μL min^{-1} with a 27-gauge stainless steel hypodermic needle. To optimize of the PEDOT:PSS thin film, five PEDOT:PSS/FTO electrodes were prepared with various deposition times, which are denoted as P1, P2, P3, P4, and P5, corresponding to deposition times of 1, 2, 3, 5, and 9 min, respectively. And then PEDOT:PSS/FTO electrodes were annealed at 80 °C under vacuum conditions for 60 min. As discerned by optical transmittance at 550 nm (**Fig. S7a**), their transmittances decreased by *ca*. 91, 84, 77, 73, and 65% in that order with respect to longer deposition time. As shown in **Fig. S7b,** conductivity and sheet resistance are optimized for the P4 electrode. **Figs. S7c** and **S7d** are the SEM images of the PEDOT:PSS/FTO (P4).

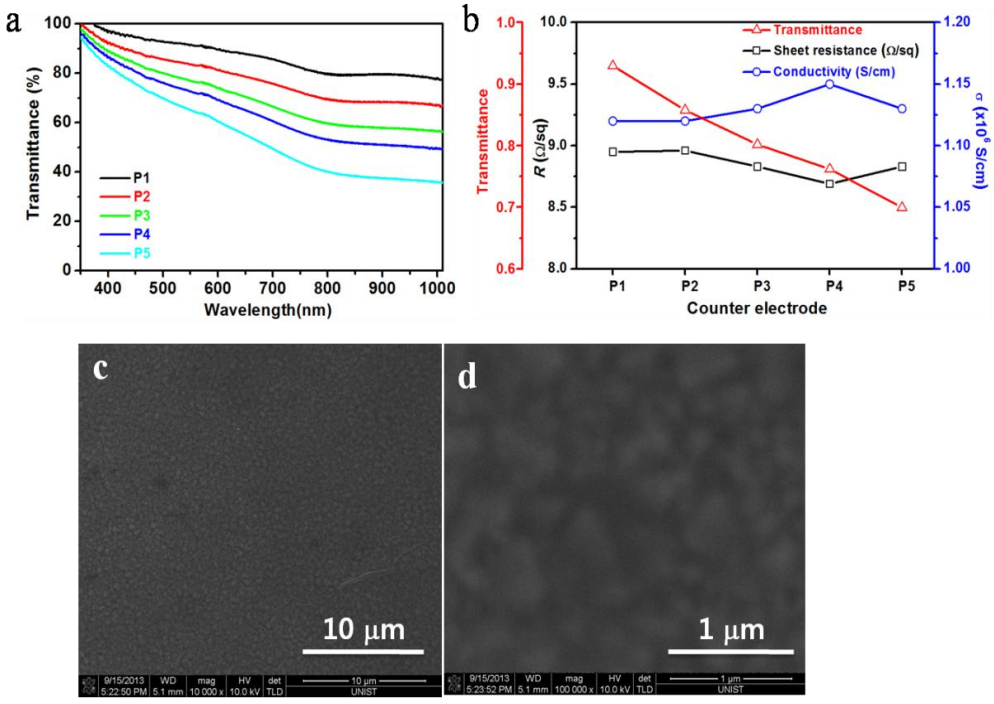

Fig. S7 (a) Optical transmittance of PEDOT:PSS films on FTO. (b) Sheet resistance and conductivity of PEDOT:PSS/FTO electrodes as a function of deposition time. SEM images of P4; scale bars of 10 μm (c) and 1 μm (d).

Fig. S8a shows the EIS spectra of the PEDOT:PSS/FTO-dummy cells for $Co(bpy)_3^{2+/3+}$ redox couple with the their numerical data summarized in **Table S1.** Unlike P1-, P2- and P4-dummy cells, EIS spectra for the P3- and P5-dummy cells exhibited three semicircles corresponding to two sequential charge-transfer processes and Nernst diffusion impedance, respectively. The equivelant circuit by the combination of two R_{CT}-CPE elements (R_{CT1}-CPE_1 and R_{CT2}-CPE_2) is connected in series (the inset in **Fig. S8a**), which may be related with the surface roughness of PEDOT:PSS on FTO judged by the decreased CPE parameter β. As shown in **Fig. S8b**, since the P4 electrode has the lowest R_{CT} (R_{CT1}+R_{CT2}) value, it can be expected to show a high FF and a PCE in the operation of the DSSCs. Subsequently, we have investigated electrocatalytic performance of the PEDOT:PSS (P4) electrodefor $Co(bpy)_3^{2+/3+}$ redox coupleas an another reference CE together with Pt electrode.

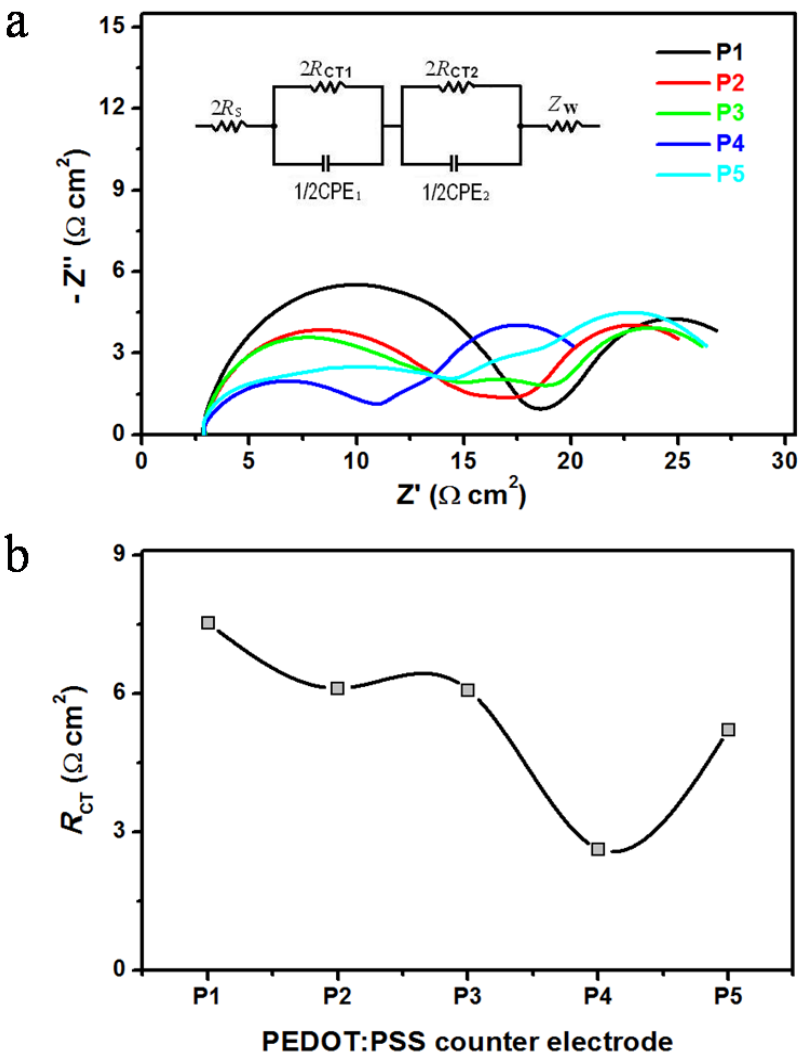

Fig. S8 (a) Nyquist plots measured at 0 V from 10^6 Hz to 0.1 Hz on the symmetrical dummy cells using PEDOT:PSS/FTO electrodes. The inset is the equivalent circuit connected with two Randles type in series. (b) R_{CT} in accordance with PEDOT:PSS/FTO-CEs.

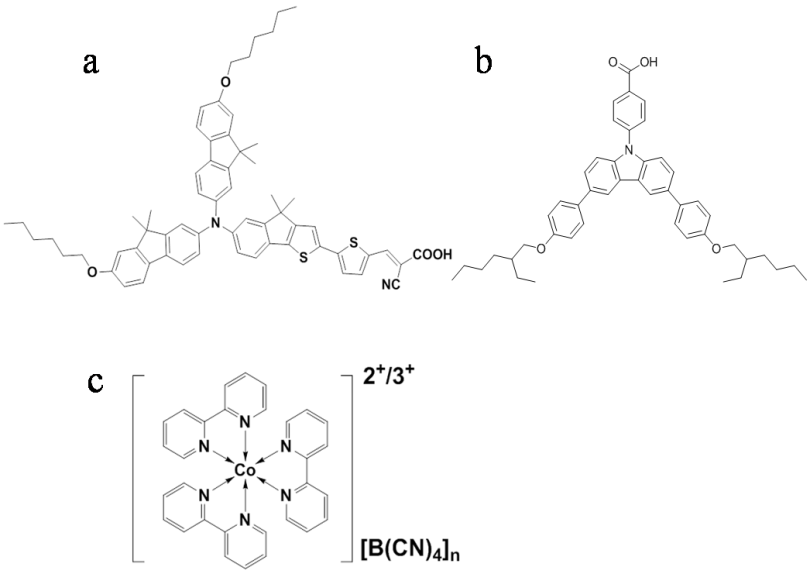

Fig. S9 Chemical formulas: (a) JK-303 dye; (b) HC-A coadsorbent (SGT-301); (c) $Co(bpy)_3^{2+/3+}$ redox couple.

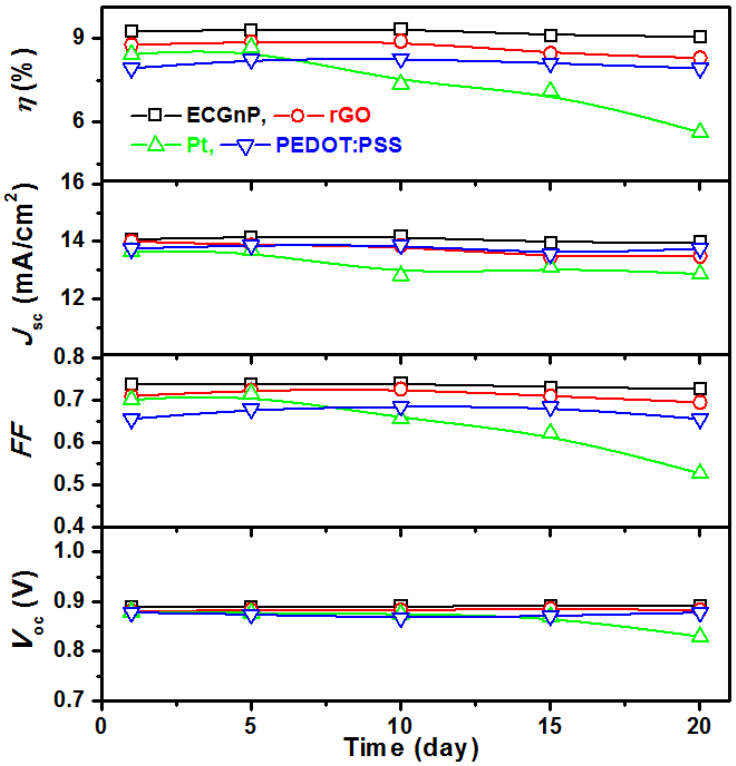

Fig. S10 Stability of the DSSCs with different CEs on storage in the dark at room temperature. Three DSSCs for each kinds of cells were tested for stability test of the DSSCs, and best cell performance showed among them depicted here. Stability of the DSSCs means electrochemical stability of counter electrode of DSSCs.

Table S1. EIS parameters of the symmetrical dummy cells using PEDOT:PSS/FTO electrodes

Sample	R_S (Ω cm^2)	R_{CT1} (Ω cm^2)	CPE$_1$:1/B (Ss$^{\beta}$)	CPE:β	R_{CT2} (Ω cm^2)	CPE$_2$:1/B (Ss$^{\beta}$)	CPE:β	R_{CT} (R_{CT1}+R_{CT2})
P1	1.34	7.53	3.91×10^{-5}	0.82	-	-	-	7.53
P2	1.31	6.11	9.49×10^{-5}	0.72	-	-	-	6.11
P3	1.34	3.86	2.91×10^{-5}	0.85	2.22	6.75×10^{-3}	0.54	6.08
P4	1.31	2.63	2.53×10^{-4}	0.66	-	-	-	2.63
P5	1.28	1.11	3.34×10^{-5}	0.89	4.10	2.50×10^{-3}	0.57	5.21

References

S1. (a) M. Liberatore, F. Decker, L. Burtone, V. Zardetto, T. M. Brown, A. Reale and A. Di Carlo, *J. Appl. Electrochem.*, 2009, **39**, 229. (b) G. Wang, W. Xing and S. Zhou, *J. Power Sources*, 2009, **194**, 568.

S2. A. Hauch and A. Georg, *Electrochim. Acta*, 2001, **46**, 3457.

S3. (a) W. Hong, Y. Xu, G. Lu, C. Li and G. Shi, *Electrochem. Commun*., 2008, **10**, 1588. (b) S. Ahmad, J-H. Yum, Z. Xianxi, M. Grätzel, H.-J. Butt and M. K. Nazeeruddin, *J. Mater. Chem*., 2010, **20**, 1. (c) H. Tian, Z. Yu, A. Hagfeldt, L. Kloo and L. Sun, *J. Am. Chem. Soc*., 2011, **133**, 9413. (d) H. N. Tsao, J. Burschka, C. Yi, F. Kessler, M. K. Nazeeruddin and M. Grätzel, *Energy Environ. Sci*., 2011, **4**, 4921.